

# Numerical Simulations of Fracture Resistance of Functionally Graded Concrete Materials

Francisco Evangelista, Jr., Jeffery Roesler, and Glaucio Paulino

The concept of grading material composition in a predetermined direction to target multiple objectives and functionality is applicable to the layering and positioning of different materials at specified depths. From a fracture mechanics perspective, this study explores the advantages of using functionally graded concrete materials (FGCMs), that is, plain concrete and fiber-reinforced concrete (FRC), in two distinct layers. The fracture energy ( $G$ ) and residual load capacity ( $P_{\delta}$ ) of two-layered concrete beams are investigated by means of numerical simulations with a cohesive zone model (CZM) implemented in a finite element framework. The required fracture parameters for defining the CZM are obtained from individual fracture tests of the plain concrete and FRC materials. The numerical simulations analyzed the effects of FRC thickness and position (whether at the top or bottom of the beam) on the fracture resistance of the two-layered concrete beam. A cost–benefit analysis showed that the FRC placed in the bottom lift is more fracture efficient (higher  $G$ - and  $P_{\delta}$ -values at lower cost) than when it is placed in the top lift. There is also an optimal FRC thickness in which the benefit in fracture resistance is reduced as the FRC layer is increased. The application of a CZM to predict the fracture behavior of an FGCM beam has demonstrated its potential for also quantifying the effects of FGCMs on the fracture resistance of concrete pavements.

For a long time, engineers and researchers have been selecting construction materials and designing a structure's geometry in an attempt to optimize cost and service life. The spatial distribution of material properties in a structural system is crucial to its structural performance under mechanical and environmental loading (1–3). Functionally graded materials (FGMs) are specifically engineered to grade the material constituents in order to define a composite whose effective mechanical properties functionally and continuously change within the material. FGMs have been extensively used in high-performance materials such as metal–ceramic and piezoelectric composites (4–9). A comprehensive review of the research and development of FGMs can be found elsewhere (5–7). The same concept of FGMs can be applied to different materials placed in bonded layers at specified thicknesses in order to meet multiple structural requirements. For example, Birman (8, 9) studied the use

of different configurations of fiber-reinforced layers to optimize the buckling resistance of composite plates and sandwich panels. Some of these concepts are extended to concrete material systems in the current work.

The addition of discrete fibers has been a reliable alternative for improving the fracture resistance of concrete materials (10–14). Originally, steel fibers were primarily employed. However, new manufactured polymeric materials, as well as byproducts, and naturally occurring fiber materials have been used to improve the cracking characteristics of concrete (15, 16). Several examples of fiber materials are polypropylene, polyethylene, carbon, nylon, bamboo, and sisal. Fiber-reinforced concrete (FRC) generally does not increase the tensile strength of the concrete at volume fractions less than 1% but does demonstrate better impact and fatigue resistance and crack width control. The ability to alter the crack growth mechanism at the material level and thus improve the global resistance of the structural system to cracking is the main benefit of adding fibers to plain concrete. This improvement is primarily due to the fibers' ability to create a large bridging zone in the concrete matrix in addition to the expected aggregate–matrix process zone. The constitutive behavior of the FRC is dependent on the fiber debonding process (fiber pullout), which is primarily related to the geometric properties of the fibers and also the mechanical properties of the concrete matrix (12, 14, 17). The characteristics of both the aggregate and fiber bridging zones produce a specific nonlinear softening behavior for a given concrete material.

Concrete pavement systems can take advantage of the principles of FGMs. The concrete materials in rigid pavements need to be designed to achieve multiple objectives, such as resistance to mechanical loads from traffic (e.g., tensile stresses at the bottom of the slab) and environmental loads (e.g., thermal and moisture gradients affecting tensile stresses at the top of the slab). To meet these overall objectives, a compositionally graded pavement structure can have layers of specific material properties placed at the optimal location and thickness to enhance the overall structural performance relative to a monolithic material placement.

The idea of using concrete placed in two functionally different layers has already been implemented in Europe (18–22) and experimented with in the United States (23, 24). These bilayer (two-lift) concrete pavement applications employ a surface concrete layer to improve frictional resistance and to attenuate the tire–pavement noise while using a conventional mixture to resist the tensile bending stress at the bottom of the slab. The application of bilayer concrete has performed adequately in Europe (19–22, 25) and demonstrates the potential for cost-effectively extending concrete pavement life or, alternatively, utilizing marginal materials strategically. Recently,

---

Department of Civil Engineering, University of Illinois at Urbana–Champaign, 205 North Mathews Avenue, MC-250, Urbana, IL 61801. Corresponding author: F. Evangelista, Jr., fevange2@illinois.edu.

*Transportation Research Record: Journal of the Transportation Research Board*, No. 2113, Transportation Research Board of the National Academies, Washington, D.C., 2009, pp. 122–131.  
DOI: 10.3141/2113-15

Roesler et al. (26) explored the structural advantages of using a two- or more layered, functionally graded concrete material (FGCM) for different combinations of plain concrete [portland cement concrete (PCC)] and fiber-reinforced concrete (FRC) material. The effective fracture behavior of the combination of these two different material layers was discussed on the basis of a series of experimental tests and numerical simulations with a finite element-based cohesive zone model (CZM).

The objective of this research is to rationally choose the placement and thickness of concrete materials in order to optimize the fracture resistance of the rigid pavement system without making the material selection cost-prohibitive. The specific analysis will address the effect of two different concrete material thickness variations and vertical position with respect to the fracture energy ( $G$ ) and the residual load capacity ( $P_s$ ) of the structure. Finite element simulations will be employed with a CZM for concrete proposed by Roesler et al. (26) and by Park et al. (unpublished work, 2008) to simulate the behavior of the plain concrete and FRC of varying thicknesses and vertical locations. Comparisons with published results will also be presented to verify the model capabilities. It is important to mention that the term FGCM is a general term in which two or more layers can be used. In this way, the two-lift pavement as already implemented in Europe and the United States is a specific case of FGCM.

### CZM FOR PLAIN CONCRETE AND FRC MATERIALS

The CZM concept was introduced by Barenblatt (27) and Dugdale (28) in order to address stress singularity at the crack tips. CZMs have been extensively used in engineering problems (29–33) because they overcome some limitations of linear elastic fracture mechanics. In these models, all nonlinearities take place in a cohesive zone ahead of the main crack tip, which is associated with the fracture process zone. Hillerborg et al. (34) applied the concept in conjunction with the finite element method to investigate concrete fracture behavior.

A CZM and the softening behavior for plain concrete and FRC, as described by Roesler et al. (26) and Park et al. (unpublished work, 2008), is shown in Figure 1. The ascending curve supports the concrete material linear elastic response before it reaches its tensile

strength ( $f'_t$ ). In the aggregate bridging zone, microcracks may grow and coalesce. In the fiber bridging zone, a variety of fiber debonding mechanisms may occur. When the crack opening displacement reaches a certain magnitude ( $w_f$ ), traction-free crack surfaces exist that correspond to a macrocrack.

The softening curve in the CZM for the PCC is physically defined by the following experimentally extracted fracture parameters: tensile strength, initial fracture energy ( $G_f$ ), total fracture energy ( $G_F$ ), and critical crack tip opening displacement (CTOD<sub>c</sub>). The initial fracture energy defines the horizontal axis intercept ( $w_1$ ) of the initial softening slope (32), expressed as follows:

$$w_1 = \frac{2G_f}{f'_t} \tag{1}$$

The determination of the kink point used here follows Park et al. (33), who postulated that the crack opening width ( $w_{k1}$ ) is given by

$$w_{k1} = \text{CTOD}_c \tag{2}$$

which results in the determination of the stress ratio ( $\psi_1$ ) at the kink point:

$$\psi_1 = 1 - \frac{\text{CTOD}_c f'_t}{2G_f} \tag{3}$$

Finally, the final crack opening width for PCC is calculated as

$$w_2 = \frac{2}{\psi_1 f'_t} [G_F - (1 - \psi_1)G_f] \tag{4}$$

which is obtained by equating the total fracture energy ( $G_F$ ) with the area under the softening model for PCC (35) and is further explained in the methodology section of this paper.

The addition of fibers increases the size of the fracture process zone by adding a fiber bridging zone behind the aggregate bridging zone. As seen in Figure 1, fibers increase the total fracture energy of the plain concrete ( $G_{\text{FRC}} \gg G_F$ ) and increase its ability to carry significant load levels in the postpeak region. The final descend-

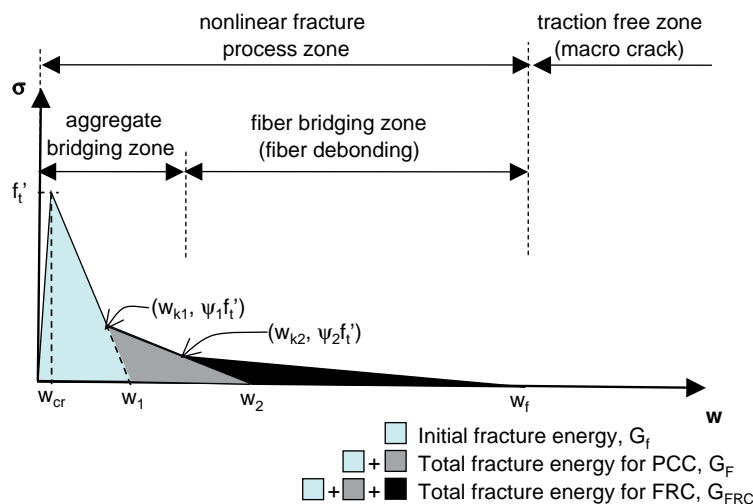


FIGURE 1 CZM and softening behavior for plain concrete (PCC) and FRC [after Roesler et al. (26) and Park et al. (unpublished work, 2008)].

ing branch of the CZM characterizes both the fiber debonding and pullout mechanisms.

One assumption used to construct the trilinear softening curve in Figure 1 for FRC materials is that the fracture parameters of the FRC are the same as the plain PCC until the first kink point. Therefore the softening model for the FRC is based partly on the plain concrete fracture parameters as explained earlier along with the FRC total fracture energy ( $G_{FRC}$ ) and  $w_f$  (here assumed as 25% of the fiber length). The second kink point ( $w_{k2}$ ) location can now be evaluated on the basis of  $G_{FRC}$  and  $w_f$ :

$$w_{k2} = w_2 - \frac{\Psi_2}{\Psi_1} (w_1 - w_{k1}) \quad (5)$$

and

$$\Psi_2 = \frac{2(G_{FRC} - G_F)}{f'_t(w_f - w_2)} \quad (6)$$

## METHODOLOGY

### Material Properties

The main objective of the research was to determine the sensitivity of the various concrete layer thicknesses and positions for the global fracture behavior of the three-point bending (TPB) beam shown in Figure 2a by using numerical simulation. Experimental properties for the plain concrete and FRC materials utilized in the simulations were extracted from work by Roesler et al. (26). A structural synthetic fiber (polypropylene–polyethylene) at a dosage of 0.78% by volume was added to the plain concrete mixture (PCC). The details about the concrete mixture design and fiber characteristics can be found elsewhere (26).

A chemical bond between the two layers was reached by mixing, casting, and consolidating the two different mixtures in the fresh state. The two-parameter fracture model (36) was employed to determine the fracture parameters for the plain concrete and FRC based on the notched TPB beam experimental test results (Figure 2b). The beam dimensions utilized for the testing and simulations are length ( $l$ ), 700 mm; span ( $s$ ), 600 mm; thickness ( $h$ ), 150 mm; width ( $w$ ), 80 mm; and notch ( $a_0$ ), 50 mm. During the TPB beam tests, the crack mouth opening displacement (CMOD) and load ( $P$ ) were measured, and

subsequently the area under the envelope curve until failure ( $P = 0$ ) was used to calculate the fracture parameters.

The total fracture energy ( $G_F$  or  $G_{FRC}$ ) was calculated on the basis of a method by Hillerborg (35):

$$G_F = \frac{W_f}{(h - a_0)w} \quad (7)$$

where  $(h - a_0)w$  is the concrete fracture area, and  $W_f$  is the total energy from the load-versus-CMOD curves ( $P$ -CMOD).

Table 1 gives the fracture parameters for the PCC and FRC mixture used in the numerical simulations. The addition of fibers did not affect the compressive strength ( $f_c$ ) of the plain concrete but did result in slightly increased split tensile strength ( $f'_t$ ) over plain concrete.

### Numerical Modeling of TPB Beam Specimen Fracture

#### TPB Beam Specimen Nomenclature

As shown in Figure 3a, the TPB beam specimen used for the simulations consists of Material 1 at the top and Material 2 at the bottom with thicknesses of  $h_{top}$  and  $h_{bottom}$ , respectively. An initial notch depth ( $a_0$ ) of 50 mm was considered for all simulations. For this specific TPB beam setup, the total beam thickness ( $h$ ) is equal to  $h_{bottom} + h_{top} + a_0$ . When the percentages of Materials 1 and 2 above the notch are equal,  $h_{bottom} = h_{top} = a_0$ . The amount of Material 2 (or 1) below the notch does not influence the fracture behavior of the TPB beam specimen, only the material contained in the ligament area,  $(h - a_0)w$ .

Numerical simulations were performed first considering the FRC position at the bottom of the TPB beam specimen. In order to present the results for different FRC thicknesses, the following relation was used:

$$FRC_{\%bottom} = \frac{h_{FRC}}{h - a_0} \times 100\% \quad (8)$$

Equation 8 provides the thickness content of the materials as the ratio of their thickness ( $h_{FRC}$  or  $h_{PCC}$ ) to the ligament depth ( $h - a_0 = h_{FRC} + h_{PCC}$ ). Figure 3b to d show the TPB beam configuration for three

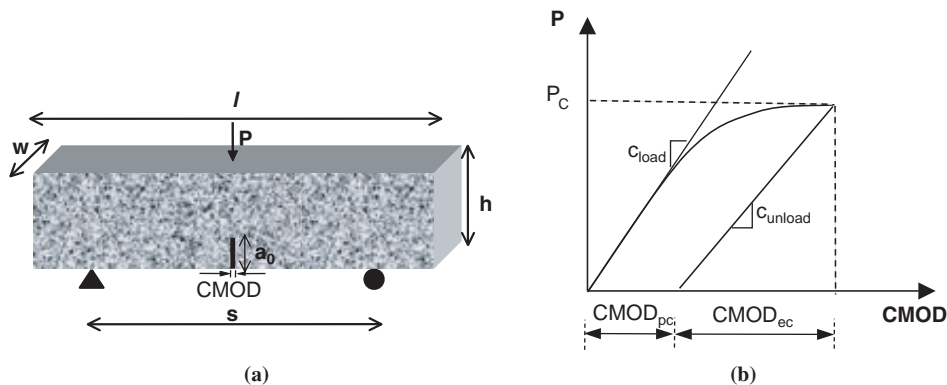
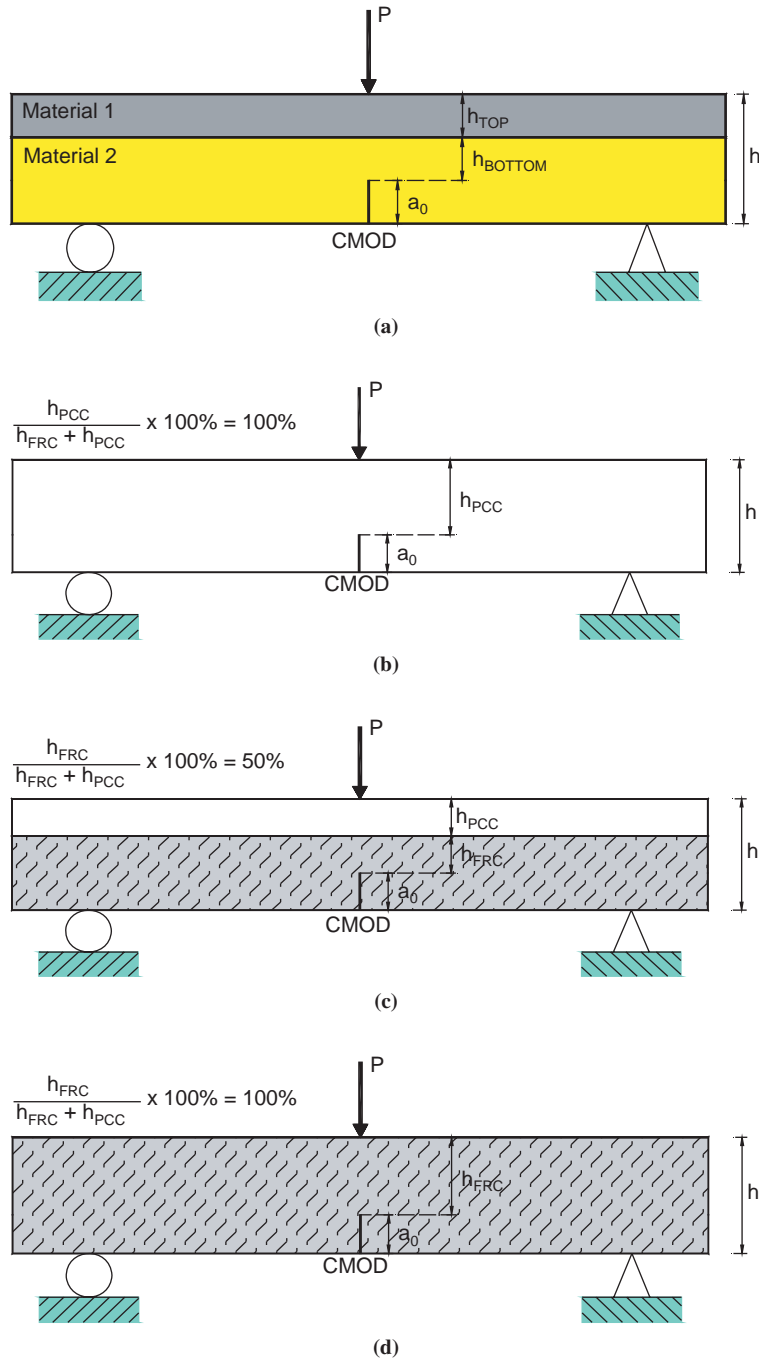


FIGURE 2 TPB beam test: (a) setup and (b) loading and unloading curves for two-parameter fracture model (36).

**TABLE 1 Mean Fracture Parameters from TPB Beam Tests for PCC and FRC (after Roesler et al. (26))**

Material	$P_c$ (kN)	$K_{Ic}$ (MPa·m <sup>1/2</sup> )	CTOD <sub>c</sub> (mm)	$G_f$ (N/m)	$a_c$ (mm)	$G_f$ or $G_{FRC}$ (N/m)	$f_c$ (MPa)	$f'_t$ (MPa)
PCC	3.710	1.05	0.016	38.1	61.8	119	28.9	3.5
FRC	3.482	1.03	0.016	36.9	66.5	3,409	28.5	4.4

NOTE:  $P_c$  = peak load for the TPB test,  $K_{Ic}$  = critical strength intensity factor in Mode I.



**FIGURE 3 TPB beam setup for (a) functionally layered concrete specimens; (b) only PCC,  $h_{FRC} = 0$  mm (0%); (c) two-layered system,  $h_{FRC} = 50$  mm (50%); and (d) only FRC,  $h_{FRC} = 100$  mm (100%).**

FRC thickness contents at the bottom (0, 50%, and 100%, respectively). Regular increments of 5 mm were used in the simulations in order to vary the thickness for the range  $0 \text{ mm} \leq h_{\text{FRC}} \leq 100 \text{ mm}$ .

Numerical simulations were also analogously considered for the FRC layer in the top lift. Similarly to Equation 8, the proportion of FRC at the top can be obtained as follows:

$$\text{FRC}_{\% \text{top}} = \frac{h_{\text{PCC}}}{h - a_0} \times 100\% \quad (9)$$

In order to report the cumulative energy absorbed at commonly accepted ranges of crack openings or widths, a cutoff criterion (e.g., 2 mm of CMOD) is used to calculate fracture energy so that relative comparisons between various thicknesses and positions can be made. The cutoff criterion is primarily needed for fibers because of their ability to effectively bridge cracks and maintain some level of residual load capacity at large values of CMOD. In this study, comparisons were made between various TPB beam specimens relative to their fracture energy ( $G_{2 \text{ mm}}$  and  $G_{3 \text{ mm}}$ ) and residual load capacity ( $P_{2 \text{ mm}}$  and  $P_{3 \text{ mm}}$ ) at 2- and 3-mm CMODs, respectively.

### Finite Element Modeling

The nonlinear softening models for PCC and FRC were implemented with the finite element method by means of a user element subroutine (Park et al., unpublished work, 2008) implemented in the commercial software ABAQUS. Figure 4 shows the mesh with the bulk elements representing the two different materials in the top and bottom layers. Shaded and unshaded areas represent different con-

crete materials. A finer mesh was used close to the crack tip in order to accurately predict the response fields. A total of 4,224 four-noded plane stress elements were used as bulk elements. Cohesive elements representing the softening response for the PCC and also FRC were placed in a predetermined vertical path above the initial notch. A total of 100 (1-mm size element) cohesive elements were used in order to accurately represent the fracture process zone, which has been shown to converge for other studies (26, 37, Park et al., unpublished work, 2008). The properties used by the cohesive element are given in Table 1. An elastic modulus of 32 GPa and Poisson's ratio of 0.19 were used for both bulk and cohesive elements.

## RESULTS AND DISCUSSION

### Load Versus CMOD ( $P$ -CMOD) Curves

Figure 5a shows the numerical  $P$ -CMOD curves for the increasing FRC thickness at the bottom as calculated from Equation 8. The curve labeled 0-FRC represents 0% of the ligament depth composed of FRC or 100% of PCC (see Figure 3b). Similarly, the  $P$ -CMOD curves labeled 50-FRC and 100-FRC in Figure 5a represent 50% and 100% of the ligament depth, as shown in Figure 3c and d, respectively. Averages of the experimental envelope curves for TPB beam specimens from the work by Roesler et al. (26) are also plotted in Figure 5a and labeled as 0-FRC test, 50-FRC test, and 100-FRC test. As expected, the peak loads were almost the same for all the simulations, and the fracture energy,  $G_{2 \text{ mm}}$  and  $G_{3 \text{ mm}}$ , increased with FRC thickness. However, for FRC thicknesses greater than 70%, the area under the  $P$ -CMOD curve is approximately the

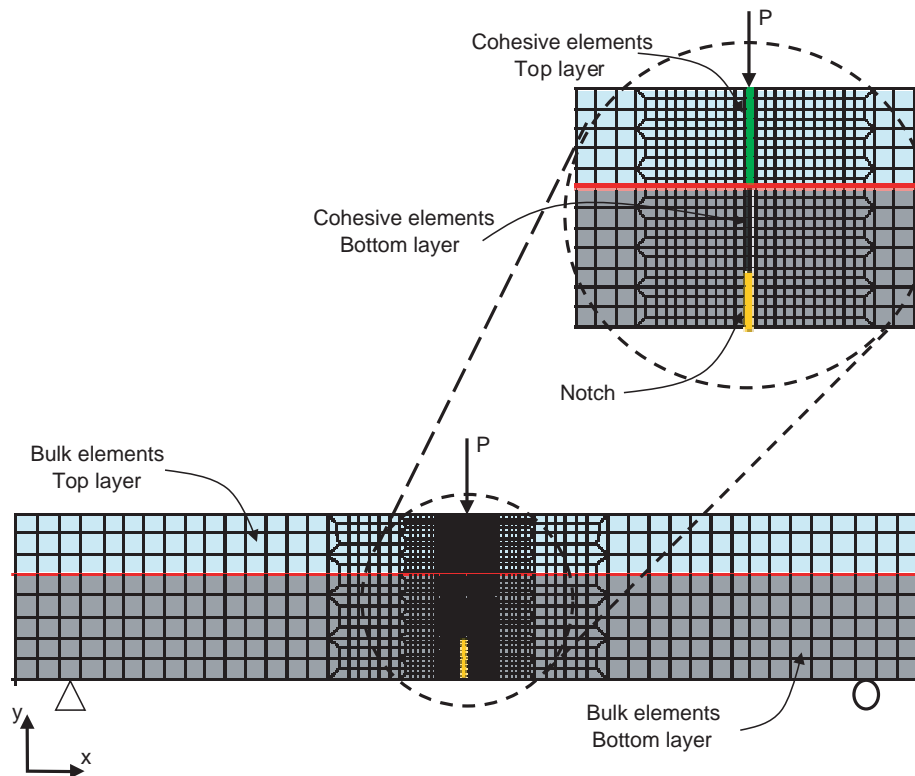


FIGURE 4 Finite element mesh with bulk and cohesive elements for two-layered beam (shaded and unshaded areas represent different concrete materials).

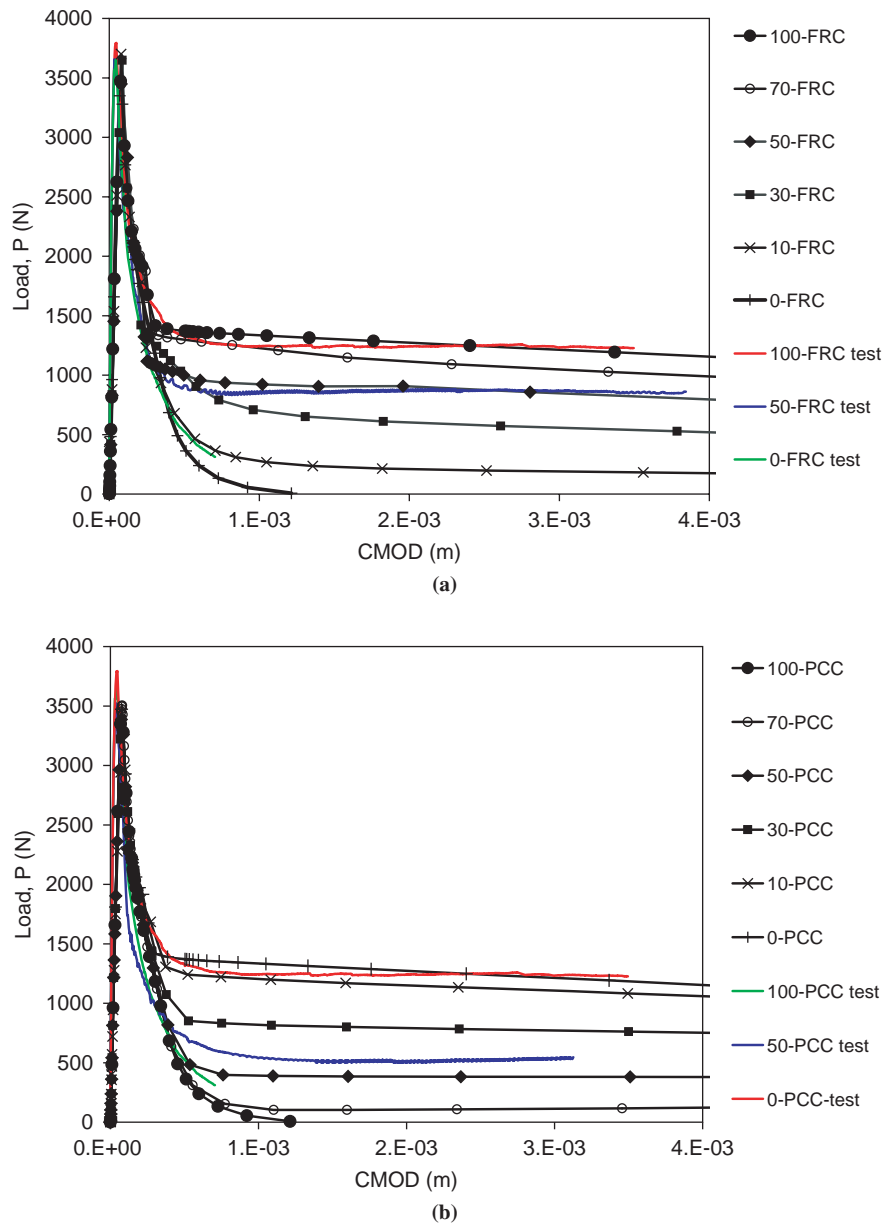


FIGURE 5 Load versus CMOD curves for different thickness content of (a) FRC at bottom of beam and (b) PCC at bottom of beam.

same, indicating that the initial increases in FRC thickness from the bottom are more important in increasing the total fracture energy of the TPB beam specimen.

Figure 5b shows the numerically simulated  $P$ -CMOD curves for the PCC at the bottom with 0-PCC, meaning that the beam ligament depth is composed of no plain concrete or 100% of FRC. Similarly, the  $P$ -CMOD curves labeled 30-PCC and 70-PCC represent 30% and 70% of the ligament depth containing PCC. Experimental results from TPB beam tests are also plotted in Figure 5b. As expected, the  $P$ -CMOD curves show that increasing  $h_{PCC}$  from the bottom toward the top of the beam decreases the fracture energies,  $G_{2\text{mm}}$  and  $G_{3\text{mm}}$ . For PCC contents greater than 70%, the area under the  $P$ -CMOD curves is similar, indicating that small thicknesses of FRC positioned at the top of the beam do not contribute significantly to global fracture resistance of the system. As illustrated in Figure 5a and b,

for the same CMOD level and FRC percentage, the most efficient position to place FRC to achieve a greater residual load capacity ( $P_\delta$ ) or fracture energy is at the bottom of the beam.

### Sensitivity of FRC Layer Thickness and Vertical Position in Beam

To analyze quantitatively the variation of the fracture energy,  $G$ , for the selected CMOD cutoff criteria (2 and 3 mm), Figure 6a shows the evolution of  $G_{2\text{mm}}$  and  $G_{3\text{mm}}$  for increasing thickness of the FRC layer for both top and bottom configurations. An increase in the thickness content of FRC at the top means less PCC thickness at the bottom. All curves indicate that a second-order polynomial can adequately fit the fracture energy versus percentage of  $h_{FRC}$ . Figure 6a

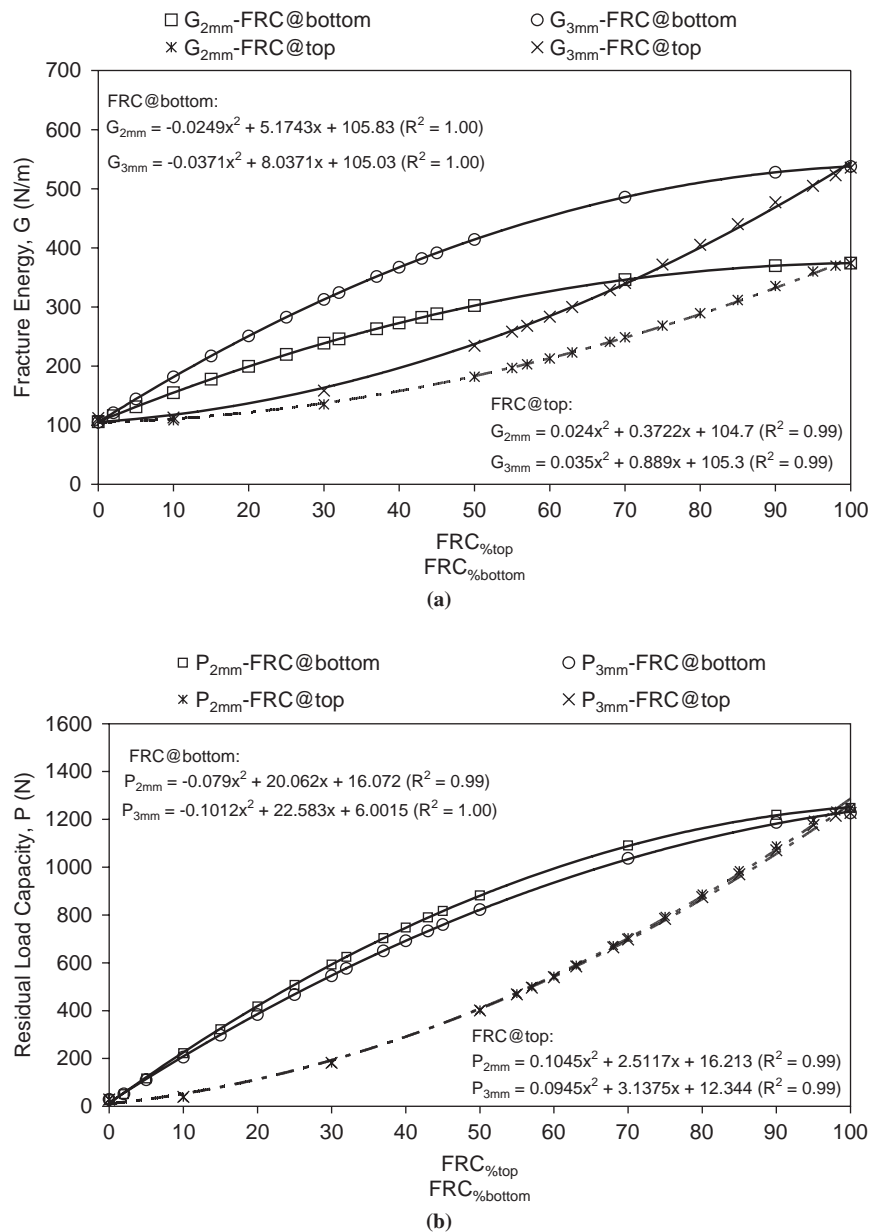


FIGURE 6 Evolution of (a) fracture energy ( $G$ ) and (b) residual load capacity ( $P_{\delta}$ ) for increasing FRC content at top or bottom of beam (solid lines represent fitted polynomial functions for FRC placed at bottom and dashed lines for FRC at top).

also shows that the FRC placed at the top is clearly less efficient (lower  $G$ -values) than the FRC at the bottom. For example, when the FRC thickness content at the top is 20%,  $G_{2mm}$  and  $G_{3mm}$  are still around 100 N/m, which is similar to the value for no FRC. When the FRC thickness content is 20% but FRC is placed at the bottom,  $G_{2mm}$  is around 180 N/m and  $G_{3mm}$  reaches 250 N/m. In Figure 6a, the difference between  $G_{2mm}$  and  $G_{3mm}$  when FRC is in the bottom versus the top lift demonstrates that the fibers are more actively engaged in resisting crack growth (pulling out).

On the basis of the same analysis used for fracture energy, Figure 6b presents the residual load capacities ( $P_{2mm}$  and  $P_{3mm}$ ) up to CMOD cutoff criteria of 2 and 3 mm, respectively. Second-order polynomials are again adequate to represent the increase of  $P_{\delta}$  with the FRC content at the top and bottom. As expected, placement of

FRC in the bottom lift of the beam maintains a much greater load capacity at 2 and 3 mm CMOD relative to FRC placed in the top lift. One difference between fracture energy and residual load capacity as a function of layer thickness content is that there is little difference between calculating  $P_{2mm}$  or  $P_{3mm}$  and thus the residual load capacity is less sensitive to the cutoff criterion selected.

The derivative of the functions ( $G'$  and  $P'$ ) shown in Figure 6 can be taken to evaluate the effectiveness of increasing the FRC bottom lift thickness on the fracture energy ( $G$ ) and residual load capacity ( $P$ ). These derivatives are plotted in Figure 7 and confirm the qualitative analyses indicating that the rate of change in  $G$  and  $P$  is greatest for initial increases in the bottom lift of FRC. As the thickness of the FRC approaches the beam thickness ( $h$ ), the payoff in increased fracture energy (Figure 7a) is reduced relative to the gain for contents

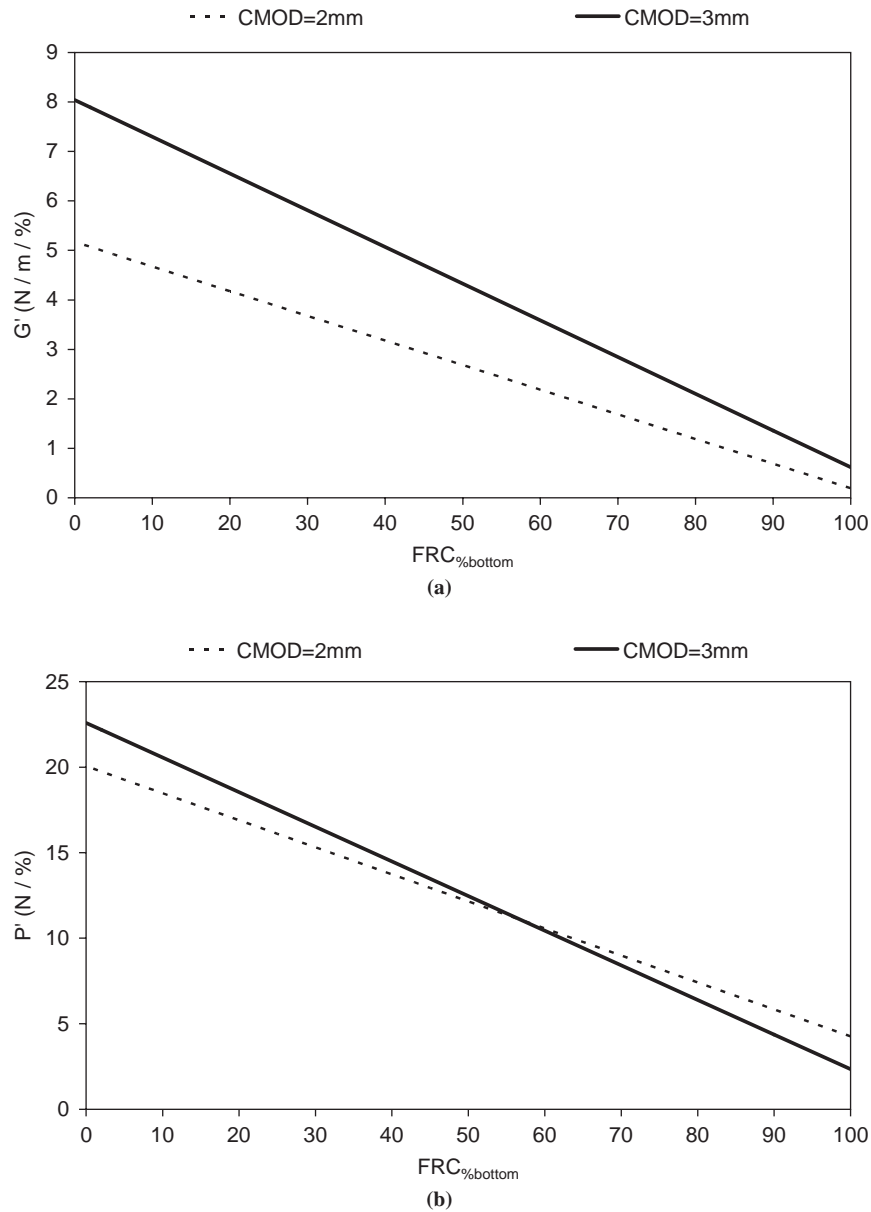


FIGURE 7 Rate of change with respect to FRC bottom lift content (%) at 2- and 3-mm CMOD of (a) fracture energy  $G'$  and (b) residual load capacity  $P'$ .

between 0 and approximately 50% of the ligament depth ( $h - a_0$ ). Figure 7b indicates that the change in residual load capacity ( $P'$ ) is also much higher for the initial increases in the bottom FRC thickness content. Like the change in fracture energy, the gain in the residual load capacity reduces as the FRC thickness approaches the total beam thickness.

### Cost-Benefit Analysis for FGCM

A cost-benefit analysis, summarized in Table 2, compares the effect of various FRC thicknesses and vertical positions on the beam fracture behavior. The structural gain (benefit) considered in this analysis is related to postpeak quantities: fracture energy ( $G$ ) and residual load capacity ( $P_\delta$ ). Enhancing those parameters are the main goals

when FRC is used. For normal strength concrete, the cost of adding fibers is assumed to increase the total concrete mixture price by 15% for this cost-benefit analysis. The cost for each beam material in Table 2 was normalized with respect to the cost of a beam with 100% of PCC. The benefit in fracture energy ( $G$ ) and residual load capacity ( $P_\delta$ ) was normalized with respect to the 100% PCC fracture energy and 100% FRC residual load capacity.

Table 2 shows an example in which 30% of the ligament depth (see Equation 8) is constructed with FRC, and the other 70% is plain concrete (PCC). The normalized cost for a beam containing 30% FRC and 70% PCC is 1.05 relative to a beam with 100% PCC. The benefit received for this 5% cost increase in terms of fracture energy at 2 mm and 3 mm CMOD is 10% and 30% higher, respectively, for the FRC positioned as the top lift. The benefits are much greater when the FRC is placed at the bottom such that  $G_{2\text{ mm}}$  and  $G_{3\text{ mm}}$

**TABLE 2 FGCM Cost–Benefit Analysis Relative to Beam Fracture Parameters  $G$  and  $P_{\delta}$**

FRC (%)	PCC (%)	Cost <sup>a</sup>	Benefit <sup>b,c</sup>			
			$G_{2\text{mm}}$	$G_{3\text{mm}}$	$P_{2\text{mm}}$	$P_{3\text{mm}}$
Top <sup>d</sup>						
0	100	1.00	1.0	1.0	0.00	0.00
10	90	1.02	1.0	1.0	0.02	0.02
30	70	1.05	1.1	1.3	0.09	0.09
50	50	1.08	1.6	2.1	0.31	0.31
70	30	1.11	2.4	3.4	0.63	0.63
90	10	1.14	3.2	4.6	0.91	0.91
100	0	1.15	3.5	5.0	1.00	1.00
Bottom <sup>d</sup>						
100	0	1.15	3.5	5.0	1.00	1.00
90	10	1.14	2.7	6.2	1.28	1.29
70	30	1.11	3.2	4.5	0.87	0.87
50	50	1.08	2.8	3.8	0.73	0.65
30	70	1.05	2.2	2.9	0.46	0.44
10	90	1.02	1.4	1.6	0.16	0.15
0	100	1.00	1.0	1.0	0.00	0.00

<sup>a</sup>Cost normalized by cost of 100% PCC. Cost of 100% FRC mixture 15% higher than 100% PCC mixture.

<sup>b</sup>Benefit to  $G$  normalized to 100% PCC fracture energy.

<sup>c</sup>Benefit to  $P$  normalized to 100% FRC residual load capacity.

<sup>d</sup>FRC layer position in the beam.

increase 2.2 (120%) and 2.8 (180%) times relative to 100% PCC. Furthermore, to reach the same  $G_{2\text{mm}}$  benefit as 30% FRC in the bottom lift, the FRC top layer must be approximately 65% of the ligament depth. For this case, the total material cost would rise from 5% to 10% above a 100% PCC beam. The residual load capacity ( $P_{\delta}$ ) for 30% FRC at the top is 9% of a full-depth beam with FRC. However, this residual load can reach 45% when the 30% FRC thickness is placed at the bottom.

## CONCLUSION

The ability to resist crack growth more efficiently by utilizing the concept of FGCMs was explored for applications to rigid pavement systems. Numerical simulations with a finite element–based CZM were performed for a TPB beam configuration containing varying thicknesses of FRC and PCC. The computational framework considered rate-independent material behavior and conglomerated all the nonlinearity due to cracking in the cohesive zone located in front of the traction-free crack tip. The sensitivity of the fracture energy ( $G$ ) and residual load capacity ( $P_{\delta}$ ) of the specimen with respect to the material configuration was determined and compared with previous experimental data. The numerical results indicated that FRC increases the fracture energy and also the residual load capacity not only when placed in the bottom lift but also when placed in the top lift. However, the FRC placed at the bottom leads to a more efficient system (higher  $G$ - and  $P_{\delta}$ -values) than when it is placed in the top lift. Furthermore, cost–benefit analysis in terms of fracture energy and residual load capacity demonstrated that increasing the FRC thickness in the bottom lift was optimal when the bottom-lift FRC

thickness was less than half of the ligament depth for these materials and test configuration.

There are obvious construction obstacles in placing two-lift systems even with the reported success of this technique in Europe, but the potential economic and pavement performance gains are encouraging. The capability of the CZM for predicting the fracture behavior of an FGCM system based on the measured fracture parameters of its individual layers enables sensitivity analyses to be completed to determine the optimal thickness and position of materials in concrete pavement to maximize cracking resistance but minimize the overall system cost.

## ACKNOWLEDGMENTS

The authors acknowledge support from the National Science Foundation. They also acknowledge Kyoungsoo Park for providing the ABAQUS user element subroutine, which implements the CZM displayed in Figure 1.

## REFERENCES

- Christensen, R. M. *Mechanics of Composite Materials*. John Wiley and Sons, New York, 1979.
- Milton, G. W. *The Theory of Composites*. Cambridge University Press, 2002.
- Goup, A. J., and S. S. Vel. Multi-Objective Optimization of Functionally Graded Materials with Temperature-Dependent Material Properties. *Materials and Design*, Vol. 28, No. 6, 2007, pp. 1861–1879.
- Hirano, T., J. Teraki, and T. Yamada. On the Design of Functionally Gradient Materials. In *Proceedings of the First International Symposium on Functionally Gradient Materials* (M. Yamanouchi, M. Koizumi, T. Hirai, and P. Shiota, eds.), Sendai, Japan, 1990, pp. 5–10.
- Paulino, G. H., Z.-H. Jin, and R. H. Dodds. Failure of Functionally Graded Materials. In *Comprehensive Structural Integrity*, Elsevier, Amsterdam, 2003, Vol. 2, Chap. 13, pp. 607–644.
- Pindera, M.-J., J. Aboudi, A. M. Glaeser, and S. M. Arnold. Use of Composites in Multi-Phased and Functionally Graded Materials. *Composites, Part B*, Vol. 28, 1997, pp. 1–175.
- Miyamoto, Y., W. A. Kaysser, B. H. Rabin, A. Kawasaki, and R. G. Ford. *Functionally Graded Materials: Design, Processing and Applications*. Kluwer Academic, Dordrecht, 1999.
- Birman, V. Stability of Functionally Graded Hybrid Composite Plates. *Composites Engineering*, Vol. 5, 1995, pp. 913–921.
- Birman, V. Stability of Functionally Graded Shape Memory Alloy Sandwich Panels. *Smart Materials and Structures*, Vol. 6, 1997, pp. 278–286.
- Balaguru, P., and S. P. Shah. *Fiber Reinforced Cement Composites*. McGraw-Hill, 1992.
- Newhook, J. P., and A. A. Mufti. Synthetic Fiber-Reinforced Concrete Bridge Decks: Redefining Bridge Deck Design and Behavior. In *Transportation Research Record 1532*, TRB, National Research Council, Washington, D.C., 1996, pp. 21–26.
- Li, V. C. On Engineered Cementitious Composites (ECC): A Review of the Material and Its Applications. *Journal of Advanced Concrete Technology*, Vol. 1, No. 3, 2003, pp. 215–230.
- Triandafilou, L. N. Implementation of High-Performance Materials: When Will They Become Standard? *Sixth International Bridge Engineering Conference: Reliability, Security, and Sustainability in Bridge Engineering* (CD-ROM), Transportation Research Board of the National Academies, Washington, D.C., 2005.
- Bentur, A., and S. Mindess. *Fibre Reinforced Cementitious Composites*, 2nd ed. Taylor and Francis, 2007.
- Cotterell, B., and Y. W. Mai. *Fracture Mechanics of Cementitious Composites*. Blackie Academic & Professional, 1996.
- Mindess, S., J. F. Young, and D. Darwin. *Concrete*, 2nd ed. Prentice Hall, 2003.

17. Yang, E. H., and V. C. Li. Fiber-Bridging Constitutive Law of Engineered Cementitious Composites. *Journal of Advanced Concrete Technology*, Vol. 6, No. 1, 2008, pp. 181–193.
18. Darter, M. I. *Report on the 1992 U.S. Tour of European Concrete Highways*. FHWA, U.S. Department of Transportation, 1992.
19. Springenschmid, R., and W. Fleischer. Recent Developments in the Design and Construction of Concrete Pavements for German Expressways (Autobahns). *Proc., Seventh International Conference on Concrete Pavements (CD-ROM)*, Orlando, Fla., 2001.
20. Fleischer, W. Concrete for Heavily Loaded Modern Traffic Areas (Part 1). *Béton*, Vol. 11, 2003, pp. 536–538.
21. van Leest, A., and W. van Keulen. The Structural Properties of Optimized Exposed Aggregate Concrete in the Netherlands. *Proc., 9th International Symposium on Concrete Roads (CD-ROM)*, Istanbul, Turkey, 2003.
22. Hall, K. *Long-Life Concrete Pavements in Europe and Canada*. Publication FHWA-PL-07-027. FHWA, U.S. Department of Transportation, 2007.
23. Smiley, D. P. *First Year Performance of the European Concrete Pavement on Northbound I-75—Detroit, Michigan*. Michigan Department of Transportation, 1995.
24. Cable, J. K., and D. P. Frentress. *Two-Lift Portland Cement Concrete Pavements to Meet Public Needs*. Technical report. FHWA, U.S. Department of Transportation, 2004.
25. Tompkins, D., L. Khazanovich, M. Darter, and W. Fleischer. Design and Construction of Sustainable Pavements: Austrian and German Two-Layer Concrete Pavements. In *Transportation Research Record: Journal of the Transportation Research Board, No. 2098*, Transportation Research Board of the National Academies, Washington, D.C., 2009, pp. 75–85.
26. Roesler, J. R., G. H. Paulino, C. Gaedicke, A. Bordelon, and K. Park. Fracture Behavior of Functionally Graded Concrete Materials for Rigid Pavements. In *Transportation Research Record: Journal of the Transportation Research Board, No. 2037*, Transportation Research Board of the National Academies, Washington, D.C., 2007, pp. 40–50.
27. Barenblatt, G. I. The Formation of Equilibrium Cracks During Brittle Fracture: General Ideas and Hypotheses, Axially Symmetric Cracks. *Journal of Applied Mathematics and Mechanics*, Vol. 23, 1959, pp. 622–636.
28. Dugdale, D. S. Yield of Steel Sheets Containing Slits. *Journal of the Mechanics and Physics of Solids*, Vol. 8, 1960, pp. 100–104.
29. Xu, X. P., and A. Needleman. Numerical Simulations of Fast Crack Growth in Brittle Solids. *Journal of the Mechanics and Physics of Solids*, Vol. 42, No. 9, 1994, pp. 1397–1434.
30. Geubelle, P., and J. Baylor. Impact-Induced Delamination of Composites: A 2D Simulation. *Composites*, Vol. 29B, 1998, pp. 589–602.
31. Song, S. H., G. H. Paulino, and W. G. Buttler. A Bilinear Cohesive Zone Model Tailored for Fracture of Asphalt Concrete Considering the Viscoelastic Bulk Material. *Engineering Fracture Mechanics*, Vol. 73, 2006, pp. 2829–2848.
32. Bazant, Z. P., and M. T. Kazemi. Determination of Fracture Energy, Process Zone Length and Brittleness Number from Size Effect, with Application to Rock and Concrete. *International Journal of Fracture*, Vol. 44, 1990, pp. 111–131.
33. Park, K., G. H. Paulino, and J. R. Roesler. Determination of the Kink Point in the Bilinear Softening Model for Concrete. *Engineering Fracture Mechanics*, Vol. 75, 2008, pp. 3806–3818.
34. Hillerborg, A., M. Modeer, and P. E. Peterson. Analysis of Crack Formation and Crack Growth in Concrete by Means of Fracture Mechanics and Finite Elements. *Cement Concrete Research*, Vol. 6, 1976, pp. 773–782.
35. Hillerborg, A. The Theoretical Basis of a Method to Determine the Fracture Energy GF of Concrete. *Material and Structures, RILEM*, Vol. 16, 1985, pp. 291–296.
36. Jenq, Y., and S. P. Shah. Two Parameter Model for Concrete. *Journal of Engineering Mechanics*, Vol. 111, No. 10, 1985, pp. 1227–1241.
37. Roesler, J. R., G. H. Paulino, K. Park, and C. Gaedicke. Concrete Fracture Prediction Using Bilinear Softening. *Cement and Concrete Composites*, Vol. 29, 2007, pp. 300–312.

---

*The Concrete Materials and Placement Techniques Committee sponsored publication of this paper.*